Wavelets to reconstruct turbulence multifractals from experimental image sequences

Pierre Dérian, Patrick Héas, Etienne Mémin

WAVELETS TO RECONSTRUCT TURBULENCE MULTIFRACTALS FROM EXPERIMENTAL IMAGE SEQUENCES

Pierre Derian
Pierre.Derian@inria.fr *

Patrick Heas
Patrick.Heas@inria.fr

Etienne Memin
Etienne.Memin@inria.fr
INRIA Rennes - Bretagne Atlantique
Campus de Beaulieu 35042 Rennes Cedex - France

ABSTRACT

In the context of turbulent fluid motion measurement from image sequences, we propose in this paper to reverse the traditional point of view of wavelets perceived as an analyzing tool: wavelets and their properties are now considered as prior regularization models for the motion estimation problem, in order to exhibit some well-known turbulence regularities and multifractal behaviors on the reconstructed motion field.

1 INTRODUCTION AND MOTIVATION ON WAVELETS AND TURBULENT MOTIONS

The fractal nature of turbulent motion fields may be derived from A. Kolmogorov statistical theory. More recently, Frisch (1995) showed how multifractal models are adapted to the description of intermittency phenomena in turbulence. These notions may be characterized by the Lipschitz regularity α or the singularity spectrum $D(\alpha)$ of a signal, resp. In this context, wavelets are known to constitute a simple yet efficient tool for regularity measurement. Given a signal, the asymptotic decay across scales of the amplitude of its wavelet coefficients can be linked to its Lipschitz regularity, under simple constraints on the analyzing wavelet. In the following, we consider a wavelet with n *vanishing moments*[1] and n fast-decay derivatives. Then, considering wavelet coefficients[2] $\{d_{j,p}\}_{j,p}$ of given function $f \in \mathbf{L}^2(\mathbb{R})$ uniformly Lipschitz $\alpha \leq n$ over the support $[0,1]$, there exist A such that (Mallat, 2008):

$$|d_{j,p}| = |\left\langle f\,,\,\psi_{j,p}\right\rangle_{\mathbf{L}^2}| \sim A(2^j)^{\alpha+1/2} \qquad (1)$$

Conversely, a bounded signal whose coefficients verify (1) for $\alpha \notin \mathbb{N}$ is uniformly Lipschitz α over $]0,1[$. Similarly, the singularity spectrum may be estimated from the computation of the partition functions of the coefficients and an inverse Legendre transform (Mallat, 2008). It has been used to exhibit the multifractal nature of turbulent velocity fields (Bacry *et al.*, 1993).

Fractality of signals is also known to reveal a power-law behavior in the power spectrum. Applied to turbulent motion, it rises up the famous -5/3 decay predicted by Kolmogorov theory. Using *continuous* wavelet transform (CWT), Perrier *et al.* (1995) define a (continuous) wavelet power spectrum (CWPS) from the energy conservation property and the multiscale nature of the CWT. At a given scale, this CWPS is proportionnal to the $\mathbf{L}^2$ norm of the wavelet coefficients. Moreover, it is related to the usual Fourier power spectrum (FPS) for a finite-energy signal. In particular, considering a power-law behavior at small scales (wavenumber $k \to \infty$) of the Fourier spectrum $E(k)$:

$$E(k) \sim k^{-\gamma}$$

then a sufficient condition for the CWPS to exhibit the *same behavior* as the FPS is to use a wavelet with $n > \frac{\gamma-1}{2}$ VM.

Aside from their use in turbulence analysis, wavelets have been employed to design motion estimators from fluid flow image sequences. Indeed, methodological advances in correlation-based or model-based measurement techniques have enhanced the accuracy of the computer-vision approach to fluid motion measurement (particle image velocimetry (Adrian, 1991), scalar imagery, meteorological or oceanographical satellite imagery (Heitz *et al.*, 2010), ...). In order to measure motion from an image sequence, any motion estimation method needs to impose either explicitly (e.g. optical flow) or implicitly (e.g. correlation) smoothness assumption on the solution through smoothness

*Authors acknowledge the support of the French Agence Nationale de la Recherche (ANR), under grant MSDAG (ANR-08-SYSC-014) "Multiscale Data Assimilation for Geophysics".

[1]The notion of vanishing moments (VM) is simply orthogonality to polynomials up to a certain order.

[2]See Sect. 2.2 for an introduction to wavelet formalism.

functions (so-called *regularizers*) or implicit parametric spatial constraints (constant, affine, etc.). Contrary to correlation-based methods, model-based techniques known as *optical flow* approaches present the advantage of offering a wide range of observation models (Liu & Shen, 2008) and regularizers, which may be chosen accordingly to the specificities of the observed flow. Authors in Heas *et al.* (2009) have designed an efficient regularization model based on statistical properties of turbulence, using the velocity increment function. More recently, a wavelet-based observation model, taking advantage of the intrinsic multiscale nature of wavelet bases, was proposed in (Dérian *et al.*, 2011). In the continuation of those works, the idea developed in this paper is to design wavelet-based regularizers to reconstruct the motion field with some desired physical properties such as fractality. Since Dérian *et al.* (2011) wavelet-based observation model relates directly wavelet coefficients of the sought motion field to image intensity variations, fractal properties on the solution can be imposed simply by constraining its wavelet coefficients decay trough scales. The wavelet framework therefore enables a much simpler and more efficient implementation of fractal regularization, and is in the same time well-adapted to optical flow estimation.

2 WAVELET-BASED OPTICAL FLOW

When addressing fluid motion estimation, one has to deal with continuous complex motion, involving a wide range of scales and velocity magnitudes. Correlation-based methods have been used successfully, especially in the context of experiments featuring flows seeded with particles (PIV). Those methods use a single data model, namely Digital Image Correlations (DIC), which is notably adapted to PIV. However, they have the drawbacks of producing sparse velocity fields, while their regularization scheme (i.e. blockwise constant fields) imposes an erroneous regularity to the reconstructed motion field. On the opposite, optical flow methods reconstruct dense motion field (i.e. one velocity vector per pixel) and offer a wide range of data models and regularizers, which can be chosen in adequacy with the specific nature of the problem. Fluid-motion-dedicated regularization schemes preserving rotational and/or divergence quantities, or built upon statistical properties of the turbulence, have been proposed. They have similar accuracy to correlations methods on PIV and outperform them on scalar transport images.

2.1 Optical Flow Problem

Optical flow aims at estimating the apparent motion field $\boldsymbol{v}(\boldsymbol{x}) = (v_1(\boldsymbol{x}), v_2(\boldsymbol{x}))^T$ transforming an image $I_0 = I(t)$ of the sequence into the next one $I_1 = I(t+1)$, $\forall \boldsymbol{x} \in \Omega$, where $\Omega \subset \mathbb{R}^2$ denotes image domain. This problem is classically solved through the minimization of a functional $J(\boldsymbol{v})$. This functional J includes a *data model* linking observed images to the sought motion fields. The simplest assumption used is the luminance consistency along a point trajectory: $\frac{dI(\boldsymbol{x}(t),t)}{dt} = 0$, which constitutes an exact physical model in the case of non-diffusive transport by bi-dimensional turbulent flows (Liu & Shen, 2008). The data model used hereafter, so-called the *Displaced Frame Difference* (DFD), is obtained by time-integration along the motion trajectories of the previous assumption:

$$\forall \boldsymbol{x} \in \Omega,\ I_0(\boldsymbol{x}) - I_1(\boldsymbol{x} + \boldsymbol{v}(\boldsymbol{x})) = 0 \tag{2}$$

The velocity field estimate $\hat{\boldsymbol{v}}$ is finally obtained by minimizing quadratic discrepancies to the data model (2):

$$\begin{cases} \hat{\boldsymbol{v}} = \arg\min_{\boldsymbol{v}} J_{\mathrm{DFD}}(\boldsymbol{v}) \\ J_{\mathrm{DFD}}(\boldsymbol{v}) = \dfrac{1}{2} \displaystyle\int_\Omega \left[I_0(\boldsymbol{x}) - I_1(\boldsymbol{x} + \boldsymbol{v}(\boldsymbol{x})) \right]^2 d\boldsymbol{x}. \end{cases} \tag{3}$$

This problem is ill-posed, as there are twice as much unknowns as equations. Moreover, this data model does not provide any information when image spatial or temporal gradients vanish. Regularization schemes are needed to circumvent those limitations.

2.2 Projection on Orthogonal Wavelet Bases

We consider the projection of each scalar component v_1, v_2 of the velocity field $\boldsymbol{v}$ onto *multi-resolution approximation spaces* exhibited by the wavelet formalism. Let us introduce briefly this context for real 1D scalar signals - see Mallat (2008) for more details. We consider a multi-resolution approximation of $\mathbf{L}^2(\mathbb{R})$ as a sequence $\{V_j\}_{j\in\mathbb{Z}}$ of closed subspaces, so-called *approximation spaces*, notably verifying:

$$V_{j+1} \subset V_j\,; \quad \lim_{j\to+\infty} V_j = \bigcap_{j=-\infty}^{+\infty} V_j = \{0\}$$

$$\lim_{j\to-\infty} V_j = \mathrm{Closure}\left(\bigcup_{j=-\infty}^{+\infty} V_j \right) = \mathbf{L}^2(\mathbb{R})$$

Since approximation spaces are sequentially included within each other, they can be decomposed as $V_{j-1} = V_j \oplus W_j$. The W_j are the orthogonal complements of approximation spaces, they are called *detail spaces*.

Practically, scalar 1D signals being finite, they belong to a given approximation space according to their resolution, i.e. number of samples. Writing $N_j = 2^{-j}\,\forall\, j \leq 0$ hereafter, let w be a 1D signal of N_{F-1} samples. Then, $w \in V_{F-1} = V_C \oplus W_C \oplus W_{C-1} \oplus \cdots \oplus W_F \subset \mathbf{L}^2([0,1])$, where $F \leq C \leq 0$. The projection of w on this multiscale basis writes:

$$\begin{aligned} w(x) = &\sum_{k=0}^{N_C-1} \langle w, \phi_{C,k} \rangle_{\mathbf{L}^2}\, \phi_{C,k}(x) \\ &+ \sum_{j=C}^{F} \sum_{k=0}^{N_j-1} \langle w, \psi_{j,k} \rangle_{\mathbf{L}^2}\, \psi_{j,k}(k) \end{aligned} \tag{4}$$

Here, $\{\phi_{C,k}\}_k$ and $\{\psi_{j,k}\}_k$ are orthonormal bases of V_C and W_j, respectively. They are defined by *dilatations* and *translations*[3] of the so-called *scaling function* ϕ and its associated *wavelet function* ψ. Finally, the representation of a signal projected onto the multiscale orthonormal wavelet basis is given by the set of coefficients appearing in (4): $a_{C,k} \triangleq \langle w, \phi_{C,k} \rangle_{\mathbf{L}^2}$ and $d_{j,k} \triangleq \langle w, \psi_{j,k} \rangle_{\mathbf{L}^2}$ are approximation and detail coefficients, respectively. Those results are extended to the case of 2D signals, in order to obtain *separable multiscale orthonormal bases* of $\mathbf{L}^2([0,1]^2)$.

2.3 Wavelet-Based Problem Formulation

In this work, we consider the wavelet expansion of each component v_i of the sought motion field $\boldsymbol{v}$; Θ_i is the set of coefficients representing v_i on the considered wavelet basis. Writing $\boldsymbol{\Theta} = (\Theta_1, \Theta_2)^T$ the superset of all coefficients, we have:

$$\boldsymbol{v}(\boldsymbol{x}) = \begin{pmatrix} v_1(\boldsymbol{x}) \\ v_2(\boldsymbol{x}) \end{pmatrix} = \begin{pmatrix} \Phi(\boldsymbol{x})\Theta_1 \\ \Phi(\boldsymbol{x})\Theta_2 \end{pmatrix} \triangleq \boldsymbol{\Phi}(\boldsymbol{x})\boldsymbol{\Theta} \tag{5}$$

Supplementing (3), the optical flow problem becomes

$$\begin{cases} \hat{\boldsymbol{v}} = \boldsymbol{\Phi}\left(\arg\min_{\boldsymbol{\Theta}} J_{\mathrm{DFD}}(\boldsymbol{\Theta})\right) \\ J_{\mathrm{DFD}}(\boldsymbol{\Theta}) = \frac{1}{2}\int_{\Omega} \left[I_0(\boldsymbol{x}) - I_1(\boldsymbol{x} + \boldsymbol{\Phi}(\boldsymbol{x})\boldsymbol{\Theta})\right]^2 d\boldsymbol{x} \end{cases} \tag{6}$$

This wavelet-based motion estimator has proven to be efficient in the context of fluid motion estimation (Dérian *et al.*, 2011), using simple regularizers (basis truncation) or more elaborate high-order regularizers.

3 RECONSTRUCTION OF TURBULENCE MULTIFRACTALS

3.1 Lipschitz Regularity

Singularity spectrum $D(\alpha)$, with α the Lipschitz regularity of a turbulent process, is related to the decay across scales of the p$^{\text{th}}$ order *partition function* (PF) of the wavelet coefficients, which is given by the p-norm of coefficients vector at a given scale. Because of the correspondence with wavelet spectrum, we consider the 2$^{\text{nd}}$ order PF defined as:

$$\mathcal{Z}(2^j) = \sum_{p=0}^{N_j - 1} \left|d_{j,p}\right|^2 \tag{7}$$

For a 2D multifractal signal, Legendre transform relates the scaling exponent of the 2$^{\text{nd}}$ order PF (power-law behavior) to its singularity spectrum - see Mallat (2008):

$$\zeta_2 = \lim_{j \to -\infty} \frac{\log_2 \mathcal{Z}(2^j)}{\log_2 2^j} = \min_{\alpha \in [\alpha_{\min}, \alpha_{\max}]} (2(\alpha+1) - D(\alpha)) \tag{8}$$

[3]Written in a general form $\psi_{j,p}(x) = 2^{-j/2}\psi(2^{-j}x - p)$.

In the case of a monofractal signal, $\zeta_2 = 2\alpha$.

3.2 Discrete Wavelet Spectrum

Similarly to relations involving continuous Fourier and wavelet spectra (Sect. 1), it is also possible to link discrete wavelet power spectrum (DWPS) to the Fourier one. For 1D signal $f \in \mathbf{L}^2([0,1])$, we define the Fourier (9) and mean wavelet (10) spectra:

$$E(k) = \frac{1}{N_F}\left|\hat{f}[k]\right|^2, \quad \forall k \in [0 \cdots N_F - 1] \tag{9}$$

$$\tilde{E}(N_j) = \frac{1}{2}\sum_{p=0}^{N_j - 1} \left|d_{j,p}\right|^2, \quad \forall j \in [-(F-1) \cdots 0] \tag{10}$$

where $\{\hat{f}[k]\}_k$ and $\{d_{j,p}\}_{j,p}$ are Fourier and wavelet coefficients, resp. Derivation of the following relation between the two spectra can be found in App. A.

$$\tilde{E}(N_j) = \frac{1}{(N_F)^2}\sum_k E(k) \left|\sum_{p=0}^{N_j - 1} \widehat{\psi}^*[(k+p)/N_j]\right|^2 \tag{11}$$

Considering a power-law behavior $k^{-\gamma}$ at small scales of FPS, it is shown in App. B that, under simple conditions on the VM of chosen wavelet, we obtain a bound on DWPS decay :

$$\begin{gathered} E(k) \sim k^{-\gamma} \text{ and } \psi \text{ with } m > \frac{\gamma+1}{2} \text{ VM} \\ \Rightarrow \tilde{E}(k) \sim k^{-(\gamma-1)} \end{gathered} \tag{12}$$

In the 2D case, the bias is of 2:

$$E(k) \sim k^{-\gamma} \Rightarrow \tilde{E}(k) \sim k^{-(\gamma-2)} \tag{13}$$

A notable difference with the CWPS relation (Sect. 1) is the apparition, in the last sum of (11), of wavelet spectrum foldings. A consequence in (12) is the bias between decays of FPS and DWPS.

3.3 Regularization Scheme

Using properties (8) and (13), we now define adequate smoothing functions for the optical flow problem exhibiting particular fractal behavior or FPS decay. Since expressions of the 2$^{\text{nd}}$ order PF (7) and the DWPS (10) are very similar, the following derivation of the regularization scheme is presented for the spectrum only. In 2D, from the hypothesis of a power-law behavior at small scales:

$$\tilde{E}(N_j) = A(2^{-j})^{-(\gamma-2)}, \forall\, F \leq j \leq L \ll 0$$

We obtain $\frac{d\log_2 \tilde{E}}{dj}(N_j) = -(\gamma - 2)$, which is approached by a finite difference. At scale 2^j, the power-law behavior finally corresponds to:

$$\frac{-1}{\gamma - 2}\left(\log_2 \tilde{E}(N_j) - \log_2 \tilde{E}(N_{j+1})\right) - 1 = 0 \qquad (14)$$

Then the constrained estimation problem writes:

$$\begin{cases} \hat{\boldsymbol{\Theta}} = \arg\min_{\boldsymbol{\Theta}} J_{\mathrm{DFD}}(\boldsymbol{\Theta}) \\ \text{s.t. } c_j(\boldsymbol{\Theta}) = (14)\ \forall F \leq j \leq L \end{cases} \qquad (15)$$

In order to exhibit a power-law of slope $-\gamma$ to the FPS, one has to pick constraints with $-(\gamma - 2)$ in 2D (13). Considering a Lipschitz regularity α for the reconstructed motion, since in 2D we have $\zeta_2 = \gamma - 2$, constraints (14) write for a monofractal with $\gamma - 2 = 2\alpha$ whereas for a multifractal $\gamma - 2 = \min_\alpha (2(\alpha+1) - D(\alpha))$ (Sect. 3.1). Note that in the latter case, we known that the minimizer is lower than $\arg\max_\alpha D(\alpha)$ - see (Mallat, 2008). Therefore, constraints apply on a point located on the left part of singularity spectrum.

3.4 Optimization

The proposed wavelet-based estimation is optimized using fast filter-banks (Dérian *et al.*, 2011). Daubechies wavelets are chosen since they have the shortest support for a given number of VM, hence minimizing computations. The algorithm processes as follows:

1. coarser (unconstrained) scales are estimated first, scale by scale, using L-BFGS (Nocedal & Wright, 1999) to achieve minimization of DFD functional;
2. to exhibit the desired property (regularity or spectrum decay), involved fine scales are also estimated, enabling constraints. Minimization of the DFD functional under constraints (15) is achieved using augmented Lagrangian method (App. C) which is appropriate here since it does not require the initialization point to respect constraints.

4 RESULTS

4.1 Synthetic PIV Dataset

Following results were obtained from a synthetic PIV image sequence generated from a 2D turbulence simulation at $Re = 3000$, using vorticity conservation equation and Lagrangian equation for non-heavy particle transported by the flow – details can be found in Carlier & Wieneke (2005). Ground truth velocity fields were thus available for evaluating the reconstruction error reduction brought by the method. Figure 1 presents an example of synthetic PIV picture, along with vorticity of the underlying simulated and estimated velocity fields. Figure 2 shows the evolution of the DWPS decay

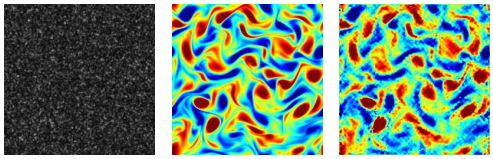

(a) (b) (c)

Figure 1: Synthetic PIV picture (*left*) used for motion estimation, along with vorticity of the underlying ground-truth motion field (*middle*) and of the reconstructed motion with proposed spectrum prior (*right*).

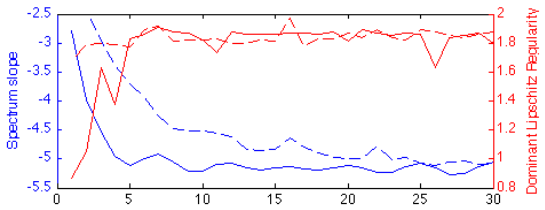

Figure 2: Analyze of *ground-truth velocity* field: evolution of the WPS slope (*continuous blue*) and dominant Lipschitz regularity α_0 (*continuous red*), as functions of the wavelet VM. WPS (compensated) slope of ground-truth converges towards the FPS slope $-\gamma = -5.05$, α_0 converges towards a median value of 1.85. Results from *motion estimation* with different VM and the proposed power-law/Lipschitz regularizations, using ground-truth values as priors: Lipschitz regularity rapidly converge towards the expected value (*dashed red*), whereas the convergence slows down with the FPS slope (*dashed blue*).

slope and dominant Lipschitz regularity, as functions of the wavelet number of VM. Slope converges towards the FPS slope of -5.05 when the analyzing wavelet has enough VM. Similarly, the estimated dominant Lipschitz regularity α_0 converges towards a median value of 1.85. Figures 3 and 4 compare power and singularity spectra, resp., of one ground-truth velocity field, of an estimate with proposed power-law regularization and of another estimate using 2^{nd} order regularization as introduced in Dérian *et al.* (2011). Note that because of the bias (13), all DWPS graphs are compensated by k^{-2} to facilitate comparisons with FPS. DWPS at scale range 2^{-5} to 2^{-7} has been constrained to decay according to a power-law of (compensated) slope $-\zeta = -5.05$, in adequacy with the slope observed on ground-truth spectra. The reconstructed FPS oscillate at finer scales, inducing a slightly lower slope decay for sufficient VM – as expected from the bound given in App. B. Root Mean Square (RMS) error on estimated motion obtained with power-law regularization is 0.086, which is to be compared with the RMS of 0.083 obtained with 2^{nd} order regularization, keeping in mind that the objective of this work is the reconstruction of statistical properties rather than RMS reduction.

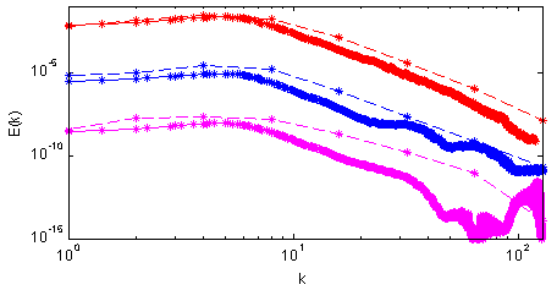

Figure 3: Comparison of FPS (*continuous*) and DWPS (*dashed lines*) obtained with a 9 VM wavelet. Graphs have been shifted vertically by 3 decades relatively so as to enhance visualization. *Red* graphs are ground-truth spectra exhibiting a power-law behavior of slope $-\alpha = -5.05$; FPS and DWPS are in good agreement. *Blue* spectra are obtained by proposed estimator with spectrum slope regularization. *Pink* graphs are obtained with 2^{nd} order regularization as presented in Dérian *et al.* (2011). Both WPS and FPS are better reconstructed by the power-law regularization (*blue*) compared to the 2^{nd} order one (*pink*), although FPS slightly oscillate at finest scales.

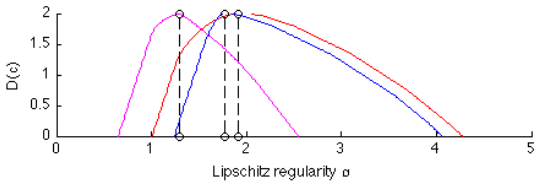

Figure 4: Comparison of singularity spectra. *Red* is obtained from ground-truth field, analyzed with a 7 VM wavelet. *Blue* results from motion estimation using ground-truth prior. *Pink* gives for comparison the spectrum of the estimate with 2^{nd} order regularization.

4.2 Scalar Diffusion

The second dataset consists in pictures of a passive scalar diffused by an electromagnetically-forced 2D turbulent motion field, investigated in Jullien *et al.* (2000). The flow features a direct enstrophy cascade, with a power-law energy spectrum $E(k) = k^{-3}$. Figure 5 shows an input image, along with the vorticity field obtained by motion estimation with a prior on the spectrum slope. Figure 6 superimposes FPS and DWPS of the estimated motion file, where PF of scales 2^{-4} to 2^{-8} are constrained to decay according to a power-law of slope $-\zeta = -3$.

CONCLUSION

An extension of wavelet-based optical flow algorithm dedicated to turbulent fluid motion estimation has been presented. Using wavelet properties, it enables the reconstruction of turbulence multifractals or power-law spectrum by controlling decay across scales of coefficients amplitude. Results on synthetic PIV as well as on experimental scalar diffusion images show enhancement brought by the proposed methodology, in terms of spectral reconstruction, in comparison to previously introduced high-order regularizers.

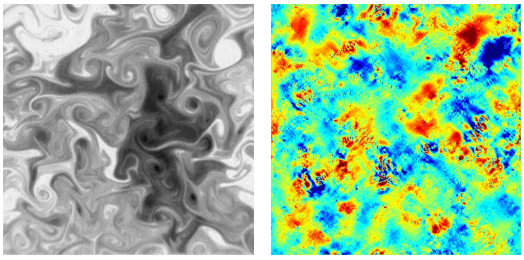

(a) (b)

Figure 5: Passive tracer diffusion picture (*left*), along with vorticity of estimated motion by optical flow with spectrum slope regularization (*right*).

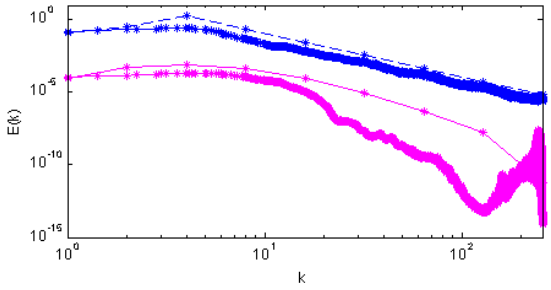

Figure 6: Comparison of FPS (*continuous line*) and DWPS (*dashed line*) of the estimated motion field obtained with a 9 VM wavelet, with a power-law behavior of slope $-\alpha = -3$ (*blue*). The vertical shift of 3 decades between blue and pink graphs has been introduced for visualization purpose. DWPS (compensated) slope is exactly -3, while FPS slope slightly deviates by $\sim 3\%$ In *pink* are given, for comparison, spectra corresponding to motion estimated using 2^{nd} order regularization, showing clearly an erroneous behavior at medium and fine scales.

References

Adrian, R. 1991 Particle imaging techniques for experimental fluid mechanics. *Annal Rev. Fluid Mech.* **23**, 261–304.

Bacry, E., Muzy, JF & Arnéodo, A. 1993 Singularity spectrum of fractal signals from wavelet analysis: Exact results. *Journal of Statistical Physics* **70** (3), 635–674.

Carlier, J. & Wieneke, B. 2005 Report 1 on production and diffusion of fluid mechanics images and data. *Fluid project deliverable 1.2. http://www.fluid.irisa.fr* .

Dérian, P., Héas, P., Herzet, C. & Mémin, E. 2011 Wavelet-based fluid motion estimation. In *3rd International Conference on Scale-Space and Varia-*

tional Methods in Computer Vision (SSVM2011). Ein-Gedi, Israel.

Frisch, U. 1995 *Turbulence : the legacy of A.N. Kolmogorov*. Cambridge university press.

Heas, P., Memin, E., Heitz, D. & Mininni, P.D. 2009 Bayesian selection of scaling laws for motion modeling in images. In *International Conference on Computer Vision (ICCV'09)*. Kyoto, Japan.

Heitz, D., Mémin, E. & Schnörr, C. 2010 Variational fluid flow measurements from image sequences: synopsis and perspectives. *Experiments in fluids* **48** (3), 369–393.

Jullien, M.C., Castiglione, P. & Tabeling, P. 2000 Experimental Observation of Batchelor Dispersion of Passive Tracers. *Physical Review Letters* **85** (17), 3636–3639.

Liu, T. & Shen, L. 2008 Fluid flow and optical flow. *Journal of Fluid Mechanics* **614**, 253.

Mallat, S. 2008 *A Wavelet Tour of Signal Processing: The Sparse Way*. Academic Press.

Nocedal, Jorge & Wright, Stephen J. 1999 *Numerical Optimization*. New York, NY: Springer-Verlag.

Perrier, V., Philipovitch, T. & Basdevant, C. 1995 Wavelet spectra compared to Fourier spectra. *Journal of Mathematical Physics* **36**, 1506.

A Discrete Wavelet Spectrum Derivation

Let f be a signal of Ω_F, i.e. with $N_F = 2^{-F}$ samples. We consider its Fourier and Wavelet transforms:

$$f[n] = \frac{1}{N_F}\sum_{k=0}^{N_F-1} \hat{f}[k]\exp^{ikn} = \sum_{-F<j\leq 0}\sum_{p=0}^{N_j-1} d_{j,p}\psi_{j,p}[n]$$

For simplicity we here considered f with a zero mean, i.e. its coarser approximation in the wavelet transform vanishes. The wavelet coefficients can be linked to the signal and wavelet Fourier coefficients:

$$\begin{aligned} d_{j,p} &= \frac{1}{\sqrt{N_F}}\left(f \star \bar{\psi}_j\right)[2^{j-F}p] \\ &= \frac{1}{N_F\sqrt{N_F}}\sum_{k=0}^{N_F-1} \widehat{f}[k]\widehat{\bar{\psi}_j}[k]\exp^{i2\pi kp/N_j} \end{aligned} \tag{16}$$

Then it is possible to link DWPS (10) to FPS (9). Wavelet coefficients are replaced by (16), then Fubini theorem allows to swap sums order.

$$\begin{aligned} \tilde{E}(N_j) &= \frac{1}{2}\sum_{p=0}^{N_j-1} |d_{j,p}|^2 \\ &= \sum_{k_1,k_2} \widehat{f}[k_1]\widehat{f}^*[k_2]\widehat{\bar{\psi}_j}[k_1]\widehat{\bar{\psi}_j}^*[k_2]\frac{N_j\delta[k_1-k_2]}{2(N_F\sqrt{N_F})^2} \\ &= \frac{N_j}{(N_F)^2}\sum_k E(k)\left|\widehat{\bar{\psi}_j}[k]\right|^2 \end{aligned} \tag{17}$$

Spectrum of the scaled wavelet $\bar{\psi}_j$ can be expressed in terms of mother wavelet spectrum. Since $\psi_j[n] \triangleq \frac{1}{\sqrt{2^j}}\psi[n/2^j]$, $j \leq 0$, using the following leads to (11).

$$\widehat{\bar{\psi}_j}[k] = \frac{1}{\sqrt{N_j}}\sum_{p=0}^{N_j-1} \widehat{\psi}^*[(k+p)/N_j] \tag{18}$$

B Power-Law Behavior

Similarly to what is done in Perrier *et al.* (1995) with continuous transforms, we consider a power-law behavior of the Fourier spectrum at large wavenumbers:

$$E(k) = k^{-\gamma}, \quad \forall\, k > k_0 \tag{19}$$

and a wavelet with m VM, which implies the existence of a continuous and bounded function ϕ such that:

$$\widehat{\psi}[k] = k^m\phi[k] \text{ and } \phi[0] = 1 \tag{20}$$

Using (19), the wavelet spectrum (17) is split in two terms at $k = k_0$, and (20) is used to replace $E(k)$ where $k > k_0$. In the limit of infinite signals ($F \to -\infty$), using Cauchy–Schwarz inequality, then Fubini theorem to swap sums and finally bounding one of the sums by its analogous continuous integral, we obtain:

$$\begin{aligned} k \leq k_0 : \tilde{E}(N_j) &\leq (N_j)^{-2m}\sum_{p=0}^{N_j-1}\sum_{k=p}^{k_0+p} k^{2m}E(k-p)\left|\phi(\frac{k}{N_j})\right|^2 \\ &\sim (N_j)^{-2m+1} \\ k > k_0 : \tilde{E}(N_j) &\leq (N_j)^{-\gamma}\sum_{p=0}^{N_j-1}\int_{\frac{k_0+p}{J}}^{+\infty}\left(\frac{y-p}{J}\right)^{-\gamma} y^{2m}\left|\phi(y)\right|^2 dy \\ &\sim (N_j)^{-\gamma+1} \text{ if } \gamma < 2m+1 \end{aligned}$$

Thus, the second term dominates when $N_j \to \infty$ if $m > \frac{\gamma}{2}$. Finally, a signal whose FPS is a power-law of slope $-\gamma$ will give a DWPS of slope steeper or equal to $-(\gamma-1)$, if previous condition on the wavelet VM is verified. Extension to the case of 2D signals gives a DWPS decay bound of $-(\gamma-2)$ for a $-\gamma$ FPS slope.

C Augmented Lagrangian

Augmented Lagrangian (AL) is related to quadratic penalty, but avoid ill-conditioning by introducing explicit Lagrange multipliers (Nocedal & Wright, 1999). From (15), AL writes at iteration k:

$$\begin{aligned} \mathcal{L}_A(\boldsymbol{\Theta}^k, \lambda^k, \mu^k) =& J_{\mathrm{DFD}}(\boldsymbol{\Theta}^k) \\ &- \sum_{j=L}^{F}\lambda_j^k c_j(\boldsymbol{\Theta}^k) + \sum_{j=L}^{F}\frac{1}{2\mu_j^k}(c_j(\boldsymbol{\Theta}))^2 \end{aligned} \tag{21}$$

Here $\{\lambda_j^k\}_j$ and $\{\mu_j^k\}_j$are respectively Lagrange multipliers and penalization factors associated to constrained scales $F \leq j \leq L$. At iteration k, minimizer $\hat{\boldsymbol{\Theta}}^k$ of functional (21) is obtained using L-BFGS method. After convergence, multipliers are updated according to $\lambda_j^{k+1} = \lambda_j^k - \frac{c_j(\hat{\boldsymbol{\Theta}}^k)}{\mu_k}$, whereas penalization factors decay according to $\mu_j^{k+1} \in [0; \mu_j^k]$; here we used $\mu_j^{k+1} = \frac{1}{3}\mu_j^k$.